Eur. Phys. J. D **42**, 125–132 (2007)
DOI: 10.1140/epjd/e2006-00276-x

THE EUROPEAN PHYSICAL JOURNAL D

Stabilizing the intensity of a wave amplified by a beam of particles

R. Bachelard[1,a], A. Antoniazzi[2], C. Chandre[1], D. Fanelli[2,3], X. Leoncini[1,4], and M. Vittot[1]

[1] Centre de Physique Théorique[b], CNRS Luminy, Case 907, 13288 Marseille Cedex 9, France
[2] Dipartimento di Energetica and CSDC, Università di Firenze, INFN, via S. Marta, 3, 50139 Firenze, Italy
[3] Department of Cell and Molecular Biology, Karolinska Institute, 17177 Stockholm, Sweden
[4] Physique des Interactions Ioniques et Moléculaires, CNRS-Université de Provence, Centre de St Jérôme, 13397 Marseille, France

Received 11 September 2006
Published online 22 December 2006 –

Abstract. The intensity of an electromagnetic wave interacting self-consistently with a beam of charged particles as in a free electron laser, displays large oscillations due to an aggregate of particles, called the macro-particle. In this article, we propose a strategy to stabilize the intensity by re-shaping the macro-particle. This strategy involves the study of the linear stability (using the residue method) of selected periodic orbits of a mean-field model. As parameters of an additional perturbation are varied, bifurcations occur in the system which have drastic effect on the modification of the self-consistent dynamics, and in particular, of the macro-particle. We show how to obtain an appropriate tuning of the parameters which is able to strongly decrease the oscillations of the intensity without reducing its mean-value.

PACS. 94.20.Wj Wave/particle interactions – 05.45.Gg Control of chaos, applications of chaos – 11.10.Ef Lagrangian and Hamiltonian approach

1 Introduction

The self-consistent interaction between an electromagnetic wave (or a set of electromagnetic waves) and a beam of charged particles is ubiquitous in many branches of physics, e.g. accelerator and plasma physics. For instance, it plays a crucial role in the Free Electron Laser (FEL), which is used to generate a tunable, coherent, high power radiations. Such devices differ from conventional lasers in using a relativistic electron beam as its lasing medium. The physical mechanism responsible for the light emission and amplification is the interaction between the beam and a wave, which occurs in presence of a magnetostatic periodic field generated in an undulator. Due to the effect of the magnetic field, the electrons are forced to follow sinusoidal trajectories, thus emitting synchrotron radiation. This initial seed, termed *spontaneous emission*, acts as a trap for the electrons which in turn amplify it by emitting coherently, until the laser effect is reached.

The coupled evolution of radiation field and N particles can be modeled within the framework of a simplified Hamiltonian picture [1]. The $N + 1$ degree of freedom Hamiltonian displays a kinetic contribution, associated with the particles, and a potential term accounting for the self-consistent coupling between the particles and the field. Hence, direct inter-particle interactions are neglected, even though an effective coupling is indirectly provided because of the interaction with the wave.

The linear theory predicts [1], for the amplitude of the radiation field, a linear exponential instability and a late oscillating saturation. Inspection of the asymptotic phase-space suggests that a bunch of particles gets trapped in the resonance and forms a clump that evolves as a single *macro-particle* localized in phase space. The untrapped particles are almost uniformly distributed between two oscillating boundaries, and populate the so-called *chaotic sea*.

Furthermore, the macro-particle rotates around a well defined center and this peculiar dynamics is shown to be responsible for the macroscopic oscillations observed for the intensity [2,3]. It can be therefore hypothesized that a significant reduction in the intensity fluctuations can be gained by implementing a dedicated control strategy, aimed at confining the macro-particle in space. As a side remark, note that the size of the macro-particle is directly related to the bunching parameter, a quantity of paramount importance in FEL context [3].

[a] e-mail: bachelard@cpt.univ-mrs.fr

[b] Unité Mixte de Recherche (UMR 6207) du CNRS, et des universités Aix-Marseille I, Aix-Marseille II et du Sud Toulon-Var; Laboratoire affilié à la FRUMAM (FR 2291); Laboratoire de Recherche Conventionné du CEA (DSM-06-35).

For example, a static electric field [4–6] can be used to increase the average wave power. While the chaotic particles are simply accelerated by the external field, the trapped ones are responsible for the amplification of the radiation field.

The dynamics can also be investigated from a topological point of view, by looking at the phase space structures. In the framework of a simplified mean field description, i.e. the so-called *test-particle* picture where the particles passively interact with a given electromagnetic wave, the trajectories of trapped particles correspond to invariant tori, whereas unbounded particles evolve in a chaotic region of phase-space. Thus, the macro-particle corresponds to a dense set of invariant tori. Our strategy is to modify the macro-particle dynamics by restoring or destroying invariant tori in selected regions of phase space.

A technique of Hamiltonian control can be used [7,8] to reconstruct additional invariant tori around the macro-particle, in order to enhance the trapping. A specific perturbation is computed, which guarantees the confinement on invariant tori of trajectories characterized by a specific energy.

In this paper, we propose a strategy to stabilize the intensity of the wave, by modifying the characteristics of the macro-particle. A (generic) one or several-parameter family of perturbations is introduced, which allows us to modify the topology of phase-space by tuning appropriately the parameters. The residue method [9,11–13] is used to identify the important local bifurcations happening in the system when the parameters are varied, by an analysis of linear stability of selected periodic orbits. This technique enables to monitor the size, gyration and internal structure of the macro-particle. An appropriate tuning of the parameters is able to strongly decrease the oscillations of the intensity without reducing its mean-value.

The paper is organized as follows: in Section 2, the test-particle model is presented. The latter provides a simple topological representation of the self-consistent interaction. In Section 3, the residue method is discussed: in particular we show how local bifurcations can generate an enlargement of the macro-particle. In Section 4, we apply the above method to re-shape both the size and the internal structure of the macro-particle. Finally, in Section 5 we draw our conclusions.

2 Dynamics of a single particle

The dynamics of the wave-particle interaction has been described in reference [1] by the N-body Hamiltonian, accounting for a kinetic contribution and an interaction term between the particles and the radiation field:

$$H_N(\{\theta_j, p_j\}, \phi, I) = \sum_{j=1}^{N} \frac{p_j^2}{2} - 2\sqrt{\frac{I}{N}} \sum_{j=1}^{N} \cos(\phi + \theta_j), \quad (1)$$

where (θ_j, p_j) are the conjugate phase and momentum of the ith particle, and (ϕ, I) stand respectively for the conjugate phase and intensity of the radiation field. Since ϕ is a phase, (ϕ, I) belongs to $\mathbb{T} \times \mathbb{R}^+$ where $\mathbb{T}$ is the one-dimensional torus. Here (θ_j, p_j) belongs to $\mathbb{T} \times \mathbb{R}$. The phase space of the system is then $\mathbb{T}^{N+1} \times \mathbb{R}^N \times \mathbb{R}^+$. We notice that there are two conserved quantities: H_N and the total momentum $P_N = I - \sum_j p_j$. We consider the dynamics given by Hamiltonian (1) on a $2N$-dimensional manifold (defined by $H_N = 0$ and $P_N = \varepsilon$ where ε is infinitesimally small).

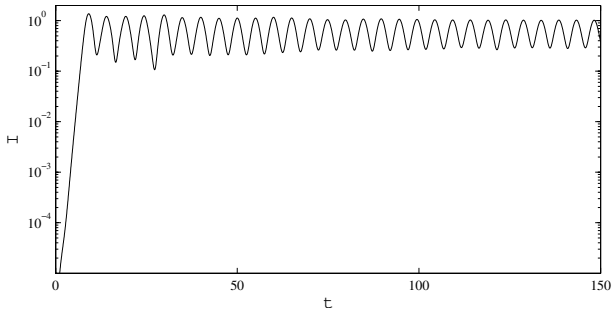

Fig. 1. Normalized intensity I/N from the dynamics of Hamiltonian (1), with $N = 10\,000$ particles and $H_N = 0$, $P_N = 10^{-7}$.

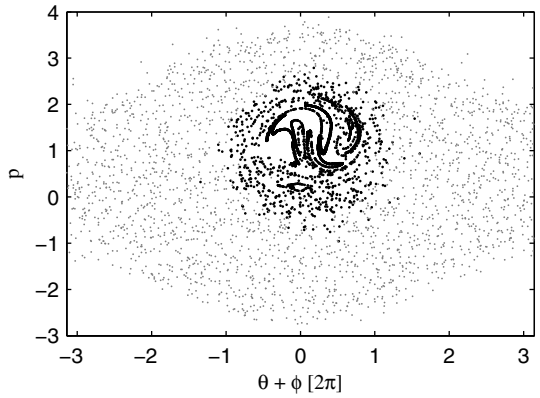

Fig. 2. Snapshot of the N particles at $t = 1000$, with $N = 10\,000$ (same parameters as Fig. 1). The grey points correspond to the chaotic particles, the dark ones to the particles in the macro-particle.

Starting from a negligible level ($I = \varepsilon$ small and $p_j = 0$), the intensity grows exponentially and eventually attains a saturated state characterized by large oscillations, as depicted in Figure 1. Concerning the particle dynamics, around half of them are trapped by the wave and form the so-called macro-particle (see Fig. 2). A particle is trapped if it travels in the potential well of the wave, after the system has reached saturation, which reads:

$$\exists k \in \mathbb{Z} \quad \text{such that} \quad \forall t \geq t_{sat}, \\ (2k-1)\pi < \theta(t) + \phi(t) < (2k+1)\pi. \quad (2)$$

The remaining particles experience a chaotic motion within an oscillating waterbag, termed chaotic sea, which is unbounded in θ contrary to the macro-particle.

In order to get a deeper insight into the dynamics, we consider the motion of a single particle. For large N, we assume that its influence on the wave is negligible, thus

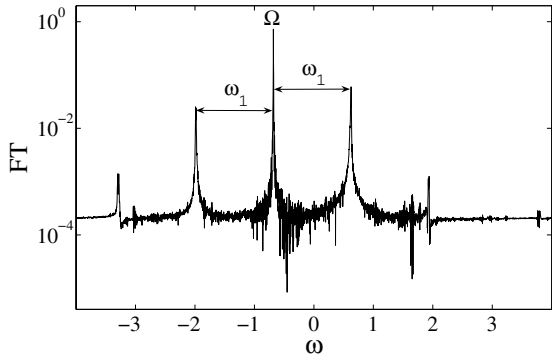

Fig. 3. Fourier transform of the interaction term $h(t)$, as obtained from simulations of Hamiltonian (1), after saturation has been reached (same parameters in Fig. 1).

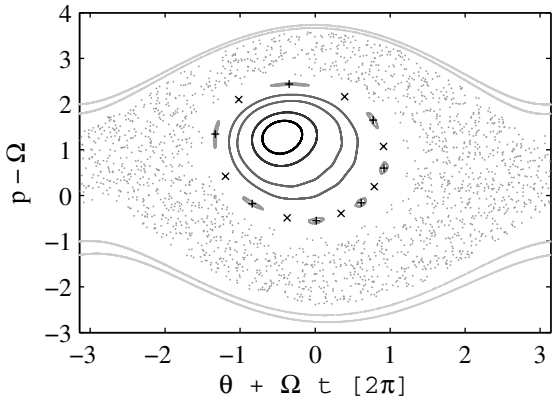

Fig. 4. Poincaré section of a test-particle, described by Hamiltonian (3). The periodic orbits with r.n. 7 are marked by plus (elliptic orbit) and crosses (hyperbolic orbit).

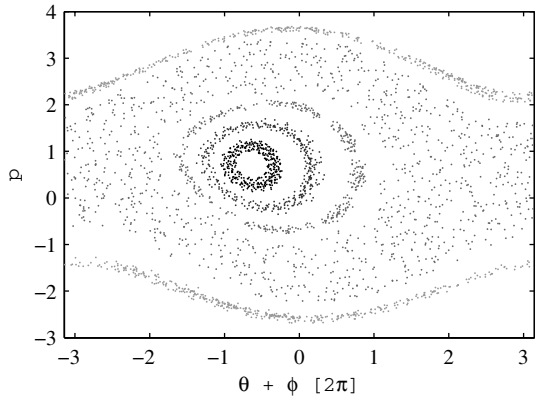

Fig. 5. Poincaré section of Hamiltonian (1), when the particles intersect the plane $dI(t)/dt = 0$. The different trajectories are represented by different grey levels.

it can be schematized as a passive particle in an oscillating field. The motion of this test-particle is described by the following Hamiltonian with one and a half degrees of freedom:

$$H_{1p}(\theta, p, t) = \frac{p^2}{2} - 2\sqrt{\frac{I(t)}{N}}\cos\left(\theta + \phi(t)\right) \quad (3)$$

$$= \frac{p^2}{2} - \mathrm{Re}\left(h(t)e^{i\theta}\right), \quad (4)$$

where the interaction term $h(t)$ is derived from some simulations of the original N-body Hamiltonian (1). In the saturated regime, $h(t)$ is mainly periodic (see Fig. 3). A refined Fourier analysis [14] shows that it can be written as:

$$h(t) = 2\sqrt{\frac{I(t)}{N}}e^{i\phi(t)} \approx [F + \alpha e^{i\omega_1 t} + \beta e^{-i\omega_1 t}]e^{i\Omega t}, \quad (5)$$

where $\Omega = -0.685$ stands for the wave velocity and $\omega_1 = 1.291$ for the frequency of the oscillations of the intensity. As for the amplitudes, the Fourier analysis provides the following values: $F = 1.5382 - 0.0156i$, $\alpha = 0.2696 - 0.0734i$ and $\beta = 0.1206 + 0.0306i$.

Hamiltonian (3) results from a periodic perturbation of a pendulum described by the integrable Hamiltonian H_0

$$H_0 = \frac{p^2}{2} - |F|\cos(\theta + \Omega t + \phi_F),$$

where $F = |F|e^{i\phi_F}$. The linear frequency of this pendulum is $\sqrt{|F|} \approx 1.240$ which is very close to the frequency of the forcing ω_1. Therefore a chaotic behaviour is expected when the perturbation is added even with small values of the parameters α and β.

The Poincaré sections (stroboscopic plot performed at frequency ω_1) of the test-particle (see Fig. 4) reveals that the macro-particle corresponds to a set of invariant tori. Conversely, the chaotic sea is filled with seemingly erratic trajectories of particles. The rotation of the macro-particle and the oscillations of the waterbag can be visualized by translating continuously in time the stroboscopic plot of the phase space.

The macro-particle is organized around a central (elliptic) periodic orbit with rotation number (r.n.) 1. The period of oscillations of the intensity is the same as the one of the macro-particle which indicates the role played by this coherent structure in the stabilization of the wave.

Thus, in the test-particle model, the macro-particle is formed by particles which are trapped on two-dimensional invariant tori. This picture can be extended to the self-consistent model, if one considers the projection of a trajectory $(\phi(t), I(t), \{\theta_j(t), p_j(t)\}_j)$ in the (θ, p) plane, each time it crosses the hyperplane $\sum_j \sin(\phi + \theta_j) = 0$, i.e. $dI/dt = 0$. From the full trajectory, we follow a given particle (an index j) and plot (θ_j, p_j) each time the full trajectory crosses the Poincaré section.

The trapped particles (following definition (2)) appear to be confined to domains of phase-space much smaller than the one of the macro-particle (see Fig. 5). These domains are similar to the invariant tori of the test-particle model, although thicker. It is worth noticing that not only these figures have a similar overall layout but there is a deeper correspondence in the structure of the macro-particle. For instance, both figures show a periodic orbit with period 7 at the boundary of the regular region. Since

we saw that the macro-particle directly influences the oscillations of the wave, the test particle Hamiltonian (3) serves as a cornerstone of our control strategy which consists in modifying the structure of the macro-particle in order to stabilize the intensity of the wave. This strategy focuses on restoring or breaking-up invariant tori to reshape the macro-particle. In order to act on invariant tori, we use the periodic orbits which, as we have seen in Figures 4 and 5 structure the macro-particle.

3 Residue method

The topology of phase space is investigated by analysing the linear stability of periodic orbits. Information on the nature of these orbits (elliptic, hyperbolic or parabolic) is provided using, e.g., an indicator like Green's residue [9,10], a quantity that enables to monitor local changes of stability in a system subjected to an external perturbation [11–13,15].

Let us consider an autonomous Hamiltonian flow with two degrees of freedom which depends on a set of parameters $\boldsymbol{\lambda} \in \mathbb{R}^m$:

$$\dot{\boldsymbol{z}} = \mathbb{J}\nabla H(\boldsymbol{z}; \boldsymbol{\lambda}),$$

where $\boldsymbol{z} = (p, E, \theta, t) \in \mathbb{R}^4$ and $\mathbb{J} = \begin{pmatrix} 0 & -\mathbb{I}_2 \\ \mathbb{I}_2 & 0 \end{pmatrix}$, and $\mathbb{I}_2$ being the two-dimensional identity matrix. In order to analyse the linear stability properties of the associated periodic orbits, we also consider the tangent flow written as

$$\frac{d}{dt} J^t(\boldsymbol{z}) = \mathbb{J}\nabla^2 H(\boldsymbol{z}; \boldsymbol{\lambda}) J^t,$$

where $J^0 = \mathbb{I}_4$ and $\nabla^2 H$ is the Hessian matrix (composed of second derivatives of H with respect to its canonical variables). For a given periodic orbit with period T, the linear stability properties are given by the spectrum of the monodromy matrix J^T. These properties can be synthetically captured in the definition of Green's residue:

$$R = \frac{4 - \mathrm{tr} J^T}{4}.$$

In particular, if $R \in]0,1[$, the periodic orbit is called elliptic (and is in general stable); if $R < 0$ or $R > 1$ it is hyperbolic; and if $R = 0$ and $R = 1$, it is parabolic while higher order expansions give the stability of such periodic orbits.

Since the periodic orbit and its stability depend on the set of parameters $\boldsymbol{\lambda}$, the features of the dynamics will change under apposite variations of such parameters. Generically, periodic orbits and their (linear or nonlinear) stability properties are robust to small changes of parameters, except at specific values when bifurcations occur. The residue method [11–13] detects the rare events where the linear stability of a given periodic orbit changes thus allowing to calculate the appropriate values of the parameters leading to the prescribed behaviour of the dynamics. As a consequence, this method can yield reduction as well as enhancement of chaos.

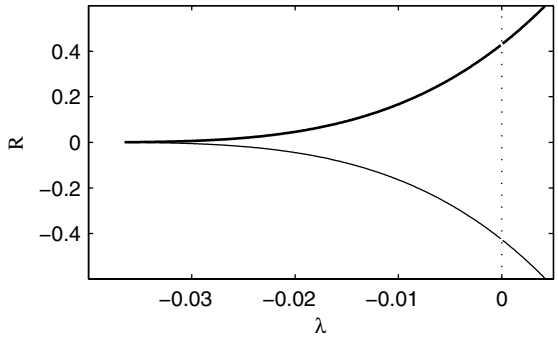

Fig. 6. Residue of the elliptic (bold curve) and hyperbolic points with r.n. 7 of Hamiltonian (3).

First, we illustrate the method by introducing an additional interaction term which depends on a parameter. The latter has to be properly tuned in order to control the dynamics. Here, the *control term* is chosen as

$$H^c_{1p}(\theta, p, t; \lambda) = H_{1p}(\theta, p, t) - 2\lambda\sqrt{\frac{I(t)}{N}}\cos\left(2\theta + \phi(t)\right), \tag{6}$$

and it is therefore similar to the original interaction term between the charged particle and the wave.

Alternatively, other types of perturbations could be selected, our choice being solely motivated by didactic reasons. For $\lambda = 0$ (which corresponds to the original Hamiltonian H_{1p}), we consider two Birkhoff periodic orbits which originates from the breakup of invariant tori with rational ratio of the integrable case (given by the nonlinear pendulum described by H_0 in the previous section). These two periodic orbits have the same action but different angles in the integrable case H_0 and have the same r.n. on the Poincaré section; one is elliptic $\mathcal{O}_e$ and one is hyperbolic $\mathcal{O}_h$ (see Fig. 4). Let us recall that the rotation number (or winding number) of a periodic orbit is the number of times it crosses the Poincaré section before closing back onto itself.

We call R_e and R_h the residues of these orbits. We have $R_e(0) > 0$ and $R_h(0) < 0$. We then modify continuously the parameter λ starting from 0. For each value of λ, we follow continuously the periodic orbit under consideration as well as its linear stability property indicated by its residue. We plot the values of the residues as a function of the parameter λ in Figure 6. We notice that at $\lambda = \lambda_c \approx -0.0370$ we have:

$$R_e(\lambda_c) = R_h(\lambda_c) = 0. \tag{7}$$

The bifurcation (7) is associated with the creation of an invariant torus [13]. This diagnostic is confirmed by the Poincaré section (see Fig. 7) of the *controlled* Hamiltonian (6), at $\lambda = \lambda_c$: the elliptic islands with r.n. 7 have been replaced by a set of invariant tori in its neighborhood, leading to an enlargement of the macro-particle. Note that elliptic islands with r.n. 5 are now present around the regular core (these orbits were present in the case $\lambda = 0$, but were both hyperbolic in the chaotic sea). The associated couple of elliptic/hyperbolic orbits

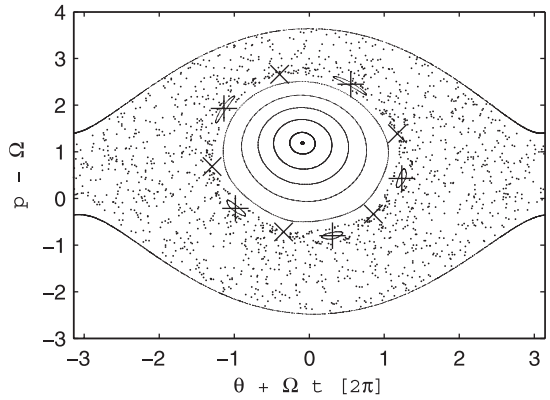

Fig. 7. Poincaré section of Hamiltonian (6) with $\lambda = \lambda_c \approx -0.0370$. The periodic orbits with r.n. 5 are marked by plus (elliptic orbit) and crosses (hyperbolic orbit).

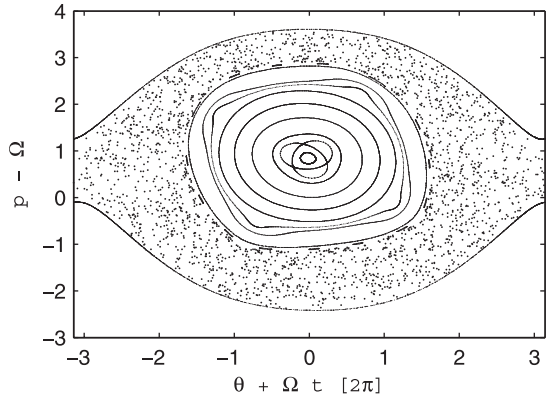

Fig. 8. Poincaré section of Hamiltonian (6) with $\lambda = \lambda_c'' \approx -0.1321$.

can be treated similarly as those of r.n. 7 in order to gain further enlargement of the macro-particle: we modify the value of the parameter λ of Hamiltonian (6) around $\lambda = \lambda_c$, until the condition (7) holds for the residues of the considered orbits. Such a condition is verified when $\lambda = \lambda_c' \approx -0.0746$, and leads to the apparition of a new set of invariant tori (not shown here); again it appears that elliptic islands with r.n. 4 surround the macro-particle. The process of increasing the size of the macro-particle can be iterated one step further. We modify the parameter λ around $\lambda = \lambda_c'$ such that condition (7) holds for the periodic orbits with r.n. 4. The residue method predicts the formation of an invariant torus at $\lambda_c'' \approx -0.1321$. Inspection of phase-space (see Fig. 8) corroborates our findings, resulting in an additional extension in size of the macro-particle.

The test-particle approach is validated using the full self-consistent Hamiltonian involving N particles (with $N \gg 1$) interacting with the wave. The control is naturally introduced in the self-consistent dynamics as:

$$H_N^c(\{\theta_j, p_j\}, \phi, I; \lambda) = H_N(\{\theta_j, p_j\}, \phi, I) - 2\lambda\sqrt{\frac{I}{N}}\sum_j \cos(2\theta_j + \phi), \quad (8)$$

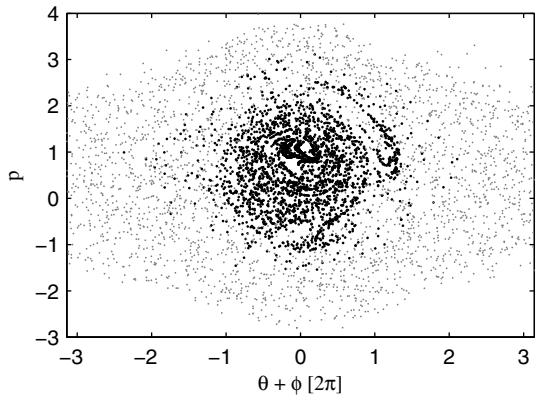

Fig. 9. Snapshot of the dynamics in the (θ, p)-plane at $t = 1000$, when Hamiltonian (8) is simulated with $N = 10\,000$ particles and $\lambda = -0.1321$. Here the control is switched on at $t = 300$, i.e. after saturation has been achieved. The grey points correspond to the particles of the chaotic sea, the dark ones form the macro-particle [see Eq. (2)].

where H_N is given by equation (1). The behaviour of the system is investigated for the three critical values where bifurcations happen in the test-particle model λ_c, λ_c', and λ_c''. For all these cases, simulations based on equation (8) display a qualitative behaviour similar to the one obtained for the original unperturbed dynamics (1): first a transient regime is detected where the intensity grows exponentially, followed by a subsequent saturation. This regime is characterized by the formation of a macro-particle whose dynamics is responsible for the oscillations observed at the intensity level. Importantly, the macro-particle is shown to increase in size also when operating within the framework of the relevant self-consistent context (see Fig. 9). In order to quantitatively characterize the evolution, we define a radius and a gyroradius associated with the inner massive aggregate. The radius corresponds to the standard deviation of the trapped particles, namely:

$$R(t) = \sqrt{\langle(\mathbf{r}_j(t) - \mathbf{r}_G(t))^2\rangle_j}, \quad (9)$$

where $\mathbf{r}_j(t) = (\theta_j(t), p_j(t))$ stands for the coordinates of the jth particle in phase-space, $\mathbf{r}_G(t) = \langle \mathbf{r}_j(t)\rangle_j$ represents the center of mass of the macro-particle, and $\langle\ \rangle_{j\in\mathcal{M}}$ denotes the average over the subset of particles constituting the inner core. On the other hand, the gyroradius characterizes the rotation of the macro-particle and reads:

$$R_{gyr} = \sqrt{\langle(\mathbf{r}_G(t) - \overline{\mathbf{r}_G})^2\rangle_{t\geq t_{sat}}}, \quad (10)$$

where $\langle\ \rangle_{t\geq t_{sat}}$ denotes an averaging over time (after saturation has been reached at t_{sat}), and $\overline{\mathbf{r}_G} = \langle \mathbf{r}_G(t)\rangle_{t\geq t_{sat}}$. As it is shown in Table 1 the radius R which is almost constant in time, increases by 28% when the control is turned on at $\lambda = \lambda_c''$, whereas the gyroradius is significantly reduced (by nearly a factor 6). These indicators points to an effective stabilization of the macro-particle dynamics in phase-space.

As reference to the wave, the control induces an effective stabilization of the intensity (see Fig. 10). In order

Table 1. Characteristics of the macro-particle and the wave for Hamiltonian (8).

λ	0	–0.037	–0.0746	–0.1321
R	0.7	0.7	0.8	0.9
R_{gyr}	0.17	0.15	0.11	0.03
$\langle I \rangle$	0.62	0.66	0.79	0.83
ΔI	0.73	0.66	0.66	0.44

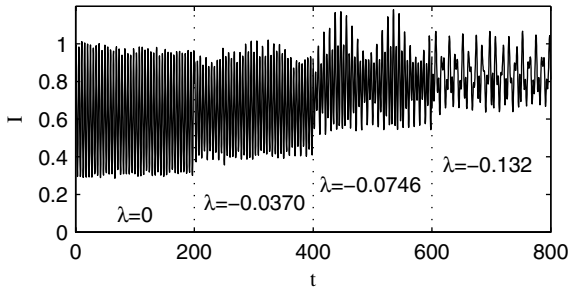

Fig. 10. Intensity of the wave in the saturated regimes for Hamiltonian (8) for four values of the parameter: $\lambda = 0$, -0.037, -0.0746 and -0.1321. For each value of λ, the system starts with a negligible value for the intensity, and a monokinetic beam of particles.

to quantify the beneficial effects of the control we measure two quantities, namely the mean value of the intensity $\langle I \rangle = \langle I(t) \rangle_{t \geq t_{sat}}$, and the average fluctuations $\Delta I = \langle |I(t) - \langle I \rangle| \rangle_{t \geq t_{sat}}$. As confirmed by inspection of Table 1 the value $\langle I \rangle$ is increased by 34% when the control is turned on, while the oscillations have damped by 39%.

4 Towards an effective stabilization of the intensity

In the previous section we provided numerical evidence that our method enables to modify the size and position of the macro-particle. Here we shall take one step further and demonstrate that we can alter the internal structure of the massive agglomerate. In particular, we will show that the macro-particle, originally composed of invariant tori, can be chaotized, thus inducing an effective mixing while keeping the particles trapped.

Information on the internal structure of the macro-particle can be gained from the residue of its central elliptic point, in the test-particle picture. In particular, the destruction of invariant tori can be expected if this orbit turns hyperbolic [13]. Thus, the residues allows one to trace the following two prescribed behaviours for the system:

1. the chaotization of the macro-particle is controlled by the residue of the central periodic point (with r.n. 1),
2. the trapping of particles is still guaranteed by the existence of invariant tori at the borders of the macro-particle (see Sect. 3).

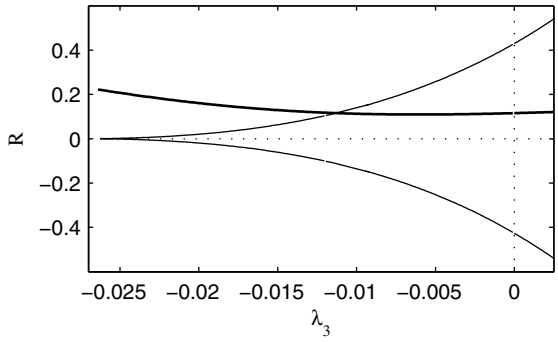

Fig. 11. Residues of the elliptic (upper curve) and hyperbolic (lower curve) points with r.n. 7, and residue of the periodic point with r.n. 1 (bold curve) of Hamiltonian (11), with all the parameters set to zero except λ_3.

To this aim, the residue method is implemented with a control term containing additional parameters. We consider the following family of Hamiltonians:

$$\tilde{H}^c_{1p}(\theta, p, t; \boldsymbol{\lambda}) = H_{1p}(\theta, p, t) - 2\sqrt{\frac{I(t)}{N}} \sum_{k=2}^{K} \lambda_k \cos\left(k\theta + \phi(t)\right), \quad (11)$$

with $\boldsymbol{\lambda} = (\lambda_2, \lambda_3 \ldots \lambda_K)$, and where H_{1p} is given by equation (3). Hence, the original system is recovered for $\boldsymbol{\lambda} = \mathbf{0}$.

First, the macro-particle is enlarged, while keeping its core composed of invariant tori: the system is perturbed by tuning the parameter λ_3 around 0; the residues of the elliptic and hyperbolic periodic orbits with r.n. 7 are monitored until condition (7) is reached at $\lambda_3^c \approx -0.0263$ (see Fig. 11), which in turn corresponds to restoring the invariant tori. Meanwhile, the residue of the central elliptic periodic point (with r.n. 1) remains stable.

The Poincaré section of Hamiltonian (11) with $\lambda_3 = \lambda_3^c$ and $\lambda_{k \neq 3} = 0$, corroborates these predictions (not shown here, but similar to Fig. 7, though the external elliptic islands have r.n. 6 instead of 5).

In order to get the macro-particle chaotic, we perturb the system (by making λ_6 different from 0) until the residue of the central elliptic orbit (of r.n. 1) crosses 0 or 1, whereas the residues of the periodic orbits of r.n. 6 satisfies condition (7).

Though the latter condition cannot be exactly matched for small values of λ_6, the residue R is shown to attain its minimal value at $\lambda_6^c = -0.0201$ (see Fig. 12), and one can expect a regularization of the dynamics in this region of phase-space. Meanwhile, the residue of the central elliptic orbit has crossed 1, so one might expect chaos in this domain. Notice that it was not possible to track numerically this central periodic orbit beyond λ_6^c. Different scenarios are compatible with this finding. Possibly the latter has been broken or alternatively it is associated with a tiny basin of attraction which prevents the multi-shooting Newton-Raphson to converge.

The Poincaré section for Hamiltonian (11) with $\lambda_3 = \lambda_3^c$, $\lambda_6 = \lambda_6^c$ and $\lambda_{k \neq 3,6} = 0$, depicted in Figure 13 displays a chaotic core, while the invariant tori of its borders are

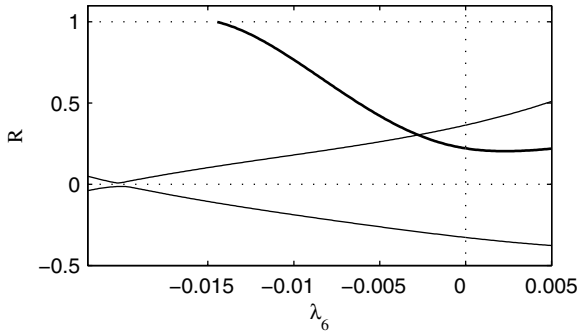

Fig. 12. Residues of the elliptic (upper curve) and hyperbolic (lower curve) points with r.n. 6, and residue of the central periodic point with r.n. 1 (bold curve) for Hamiltonian (11) with $\lambda_3 = \lambda_3^c$ and $\lambda_{k\neq 3,6} = 0$ as functions of λ_6.

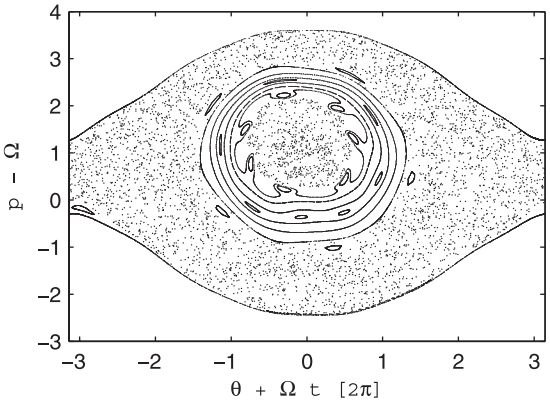

Fig. 13. Poincaré section of Hamiltonian (11) with $\lambda_3 = -0.0263$, $\lambda_6 = -0.0201$ and $\lambda_{k\neq 3,6} = 0$.

preserved, ensuring that the particles remain trapped. We have computed the Lyapunov exponents in the different regions of phase space: inside the macro-particle it is equal to 0.06 whereas, in the chaotic sea it is 0.14, i.e., more unstable.

In order to complete the analysis, a set of simulations are performed within the self-consistent framework where N particles interact with the wave. The additional perturbation is naturally introduced as:

$$\tilde{H}_N^c(\{\theta_j, p_j\}, \phi, I; \boldsymbol{\lambda}) = H_N(\{\theta_j, p_j\}, \phi, I) - 2\sqrt{\frac{I}{N}} \sum_{k,j} \lambda_k \cos(k\theta_j + \phi), \quad (12)$$

where H_N is given by equation (1). Simulations in the two regimes of control, ($\lambda_3 = \lambda_3^c, \lambda_{k\neq 3} = 0$) and ($\lambda_3 = \lambda_3^c, \lambda_6 = \lambda_6^c, \lambda_{k\neq 3,6} = 0$), confirm the prediction of the mean-field framework: the macro-particle has been increased and homogenized (see Fig. 14).

According to our estimates, the radius has been increased by more than 50%, while its gyroradius has been decreased by two orders of magnitude (see Tab. 2). As for the intensity of the wave (see Fig. 15), the fluctuations have been reduced by a factor 40, while the mean-value has been raised by 50%.

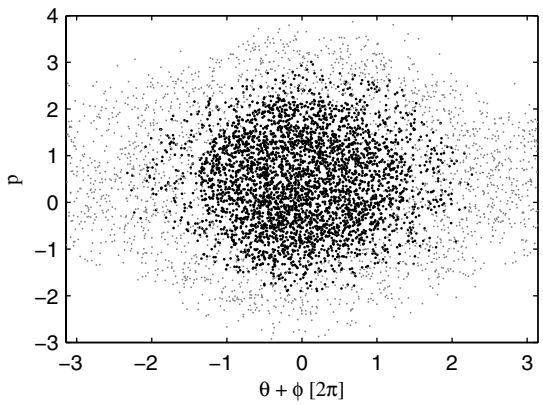

Fig. 14. Snapshot of the dynamics in the (θ, p)-plane of the $N = 10\,000$ particles at $t = 1000$ (the control started at $t = 300$) for Hamiltonian (12) with $\lambda_3 = -0.0263$ and $\lambda_6 = -0.0201$. The control term is applied at $t = 300$, after saturation has occurred. The grey points correspond to the particles of the chaotic sea, the dark ones form the macro-particle.

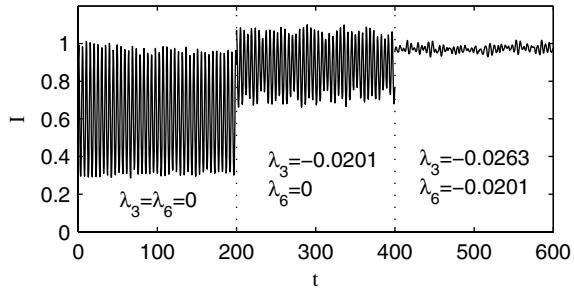

Fig. 15. Intensity of the wave in the saturated regime for Hamiltonian (12) with $\lambda_{k\neq 3,6} = 0$. For each value of $\boldsymbol{\lambda}$, the system starts with a negligible value for the intensity, and a monokinetic beam of particles.

Table 2. Characteristics of the macro-particle and the wave for Hamiltonian (12) with $\lambda_{k\neq 3,6} = 0$.

λ_3	0	–0.0263	–0.0263
λ_6	0	0	–0.0201
R	0.7	1.15	1.22
R_{gyr}	0.17	0.03	0.0015
$\langle I \rangle$	0.62	0.88	0.97
ΔI	0.73	0.44	0.017

In terms of topology of phase-space, it is interesting to observe that the regularization of the dynamics is also found within the framework of the original self-consistent picture (see Fig. 16). Indeed, the confinement of the trapped particles for Hamiltonian (11) to small domains of phase-space is more pronounced than in the unperturbed case of Hamiltonian (1).

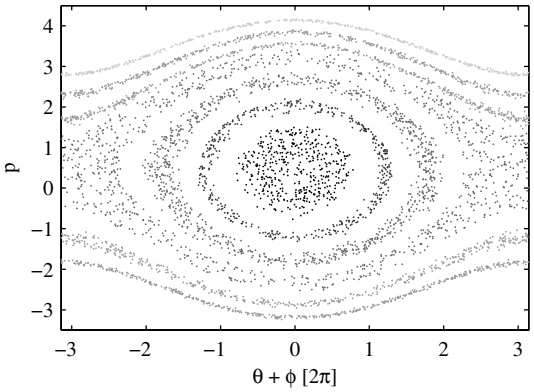

Fig. 16. Poincaré section of Hamiltonian (12) with $\lambda_3 = -0.0263$ and $\lambda_6 = -0.0201$, when the trajectory intersects the plane $dI(t)/dt = 0$. The different trajectories are represented by different grey levels.

5 Conclusion

In this paper, we proposed a stabilization strategy in a wave-particle system and in particular in the a FEL setting. The technique uses an appropriate perturbation of the associated microscopic dynamics. We carried out our approach in the saturated regime of this system where the macro-particle, resulting from a set of invariant tori, plays a crucial role. In the framework of a mean-field approximation, a linear stability analysis of selected periodic orbits (coined by a residue method) can point at the creation and destruction of invariant tori, allowing to reshape the macro-particle through specific values of the parameters of the additional perturbation. Numerical simulations performed for the original N-body self-consistent picture confirm the validity of the proposed approach and clearly demonstrate that the method allows one to predict a set of parameters for which a significant reduction of the oscillations of the intensity is found. Note that the residue method is quite flexible and applies to any two degree of freedom Hamiltonian systems. We expect that other families of perturbation terms would yield similar results.

As a final remark, we observed that the chaotization of the center of the macro-particle (by a bifurcation of the central elliptic periodic orbit which organizes the macro-particle) is associated with a strong stabilization of the intensity.

This work is supported by Euratom/CEA (contract EUR 344-88-1 FUA F). We acknowledge useful discussions, comments and remarks from G. De Ninno, Y. Elskens and the Nonlinear Dynamics team at CPT.

References

1. R. Bonifacio et al., Riv. Nuovo Cim. **3**, 1 (1990)
2. J.L. Tennyson, J.D. Meiss, P.J. Morrison, Physica D **71**, 1 (1994)
3. A. Antoniazzi, Y. Elskens, D. Fanelli, S. Ruffo, Eur. Phys. J. B **50**, 603 (2006)
4. S.I. Tsunoda, J.H. Malmberg, Phys. Rev. Lett. **49**, 546 (1982)
5. G.J. Morales, Phys. Fluids **23**, 2472 (1980)
6. A.T. Lin, Phys. Fluids **24**, 316 (1981)
7. C. Chandre, M. Vittot, G. Ciraolo, Ph. Ghendrih, R. Lima, Nucl. Fusion **46**, 33 (2006)
8. R. Bachelard, A. Antoniazzi, C. Chandre, D. Fanelli, M. Vittot, Comm. Nonlinear Sci. Num. Simu. (in press, 2006)
9. J.M. Greene, J. Math. Phys. **20**, 1183 (1979)
10. R.S. MacKay, Nonlinearity **5**, 161 (1992)
11. J. Cary, J.D. Hanson, Phys. Fluids **29**, 2464 (1986)
12. J.D. Hanson, J. Cary, Phys. Fluids **27**, 767 (1984)
13. R. Bachelard, C. Chandre, X. Leoncini, Chaos **16**, 023104 (2006)
14. J. Laskar, *Proc. of NATO ASI Hamiltonian Systems with Three or More Degrees of Freedom*, edited by C. Simò (Kluwer, Dordrecht, 1999), p. 134
15. J.E. Howard, R.S. MacKay, J. Math. Phys. **28**, 1036 (1987)